Investigation of a Buoyant Bubble Motion in a Wall-Driven Square Cavity

Ayoub Afass[1(✉)], Josep M. Bergadà[2], Soufiane Derfoufi[1], Mohammed Ahachad[1], and Mustapha Mahdaoui[1]

[1] ETTE/FSTT, Abdelmalek Essaâdi University, Tetouan, Morocco
{aafass,sderfoufi,mahachad,mmahdaoui}@uae.ac.ma
[2] Department of Fluid Mechanics, Universitat Politécnica de Catalunya, 08034 Barcelona, Spain
josep.m.bergada@upc.edu

Abstract. Direct steam generation is considered as a potential substitute for conventional power generation technologies, for its advantageous characteristics. It can be directly powered by solar radiation by concentrating it on a specific point, besides eliminating heat exchangers and fluid refrigerant, which allows to reduce operating costs. It is crucial, to properly grasp the two-phase flow involved in these technologies. In this paper, we numerically explore the effect of flow strength and wall-driven position on the flow structure and dynamic behavior of bubbles in a square enclosure, through employing the Boltzmann pseudopotential lattice method. The terminal position of the bubble reflects the concurrence between the existing forces. When the value of the Reynolds number exceeds 600, the fluid flow strength overcomes buoyancy and pushes the bubble towards the center of the primary vortex, regardless of the wall-driven configuration. In terms of flow structure, wall-driven flow structures dominate the square cavity in all studied cases. The wall motion configuration affects the bubble trajectory, especially the left wall-driven case where the bubble only reaches the second quarter of the cavity height before being driven toward the center of the primary vortex. Note that the wall configuration has a strong impact on bubble trajectory for equal Reynolds values.

Keywords: Solar energy · Direct steam generation · Lattice Boltzmann · Phase change

1 Introduction

Given the abundance of global solar irradiation, a variety of solar energy technologies are available, including concentrated solar power, solar water heating systems, central tower systems, parabolic troughs, and parabolic channels [1]. The deployment of these kinds of systems has the potential to offer pragmatic and reasonable solutions that help individuals and their environment, by supplying an alternative to fossil energy [2]. Nevertheless, the performance of solar-based systems is still rather low compared to fossil-based energy sources. Therefore, several studies have focused on the enhancement and improvement

F. Ali-Toudert et al. (Eds.): JITH 2022, LNME, pp. 333–341, 2024.
https://doi.org/10.1007/978-3-031-43934-6_34

of solar-based systems [3–5]. Nowadays, direct steam generation is considered one of the most efficient forms of concentrated solar thermal energy exploitation, especially when compared to linear Fresnel reflectors, central tower systems, and parabolic troughs [2, 6]. This excellent performance is related to the ability of liquid-vapor systems to operate at very high temperatures [6, 7]. Two-phase flow is a complex phenomenon involving multiple flow regimes ranging from bubble flow to spray flow [8]. Through optimization the channel size and mass flow rate, it is possible to maintain the bubble flow mode, which is sought in this system [1]. The work of Pal et al. [6] shows the ability of the Two-Fluid Method (TFM) to handle numerically a system of this nature, despite the presence of the Ledinegg two-phase flow instability.

In reality, two-phase flow is a widespread phenomenon, found both in nature and in industrial processes. Understanding the behavior of two-phase flow turns complex when multiple forces are involved [9, 10]. However, the Lattice Boltzmann pseudopotential method can generate a trustworthy result under these conditions. Through its results, control and prediction of equipment performance can be improved [11]. The Lattice Boltzmann Method (LBM), considered as a mesoscopic approach is based on the principle of the kinetic theory described by the original Boltzmann equation [12, 13]. The methodology used by the LBM entails the assumption that a fluid is formed by a large number of virtual particles that have undergone repeated collisions and streaming. Resulting in microscopic kinetic principles being conserved in a way that recovers the macroscopic scale hydrodynamic behavior [12, 14]. Many numerical models have been developed since the 1990s to study multiphase flows using the LBM method. One of the robust two-phase Lattice Boltzmann models is the pseudopotential model. Shan and Chen [15] initially formulated their two-phase model in early 90s with full discretization and validation. Later, some improvements are made to make it in the current form named the improved MRT pseudopotential [9, 16], the latter is used in this study. In order to predict and control the motion of the deformable bubble, the current study describes the motion of a buoyant bubble within a single wall-driven square cavity.

2 Methodology

2.1 Physical Model

This work consists of examining the effect of a wall-driven flow strength and placement on the flow topology and bubble behavior. The physical domain consists of an immersed bubble in a liquid phase of saturated water at the temperature of 0.7 T_c. Initially, the bubble center is placed in the lower part of the 2D square cavity (0.5L, 0.1L). The effect of the Reynolds number is investigated for two configurations: the upper wall is moving in the direction of positive x (Fig. 1a) and the left vertical wall is moving upward (Fig. 1b). The domain was initially allowed to stabilize in a free gravity field for 10000-time steps, then gravity and a flow motion were triggered. The gravitational acceleration is set at $g = 2 \times 10^{-5}$ lu ts^{-2} and the wall-driven flow is ensured by varying the Reynolds number in the range [300, 900].

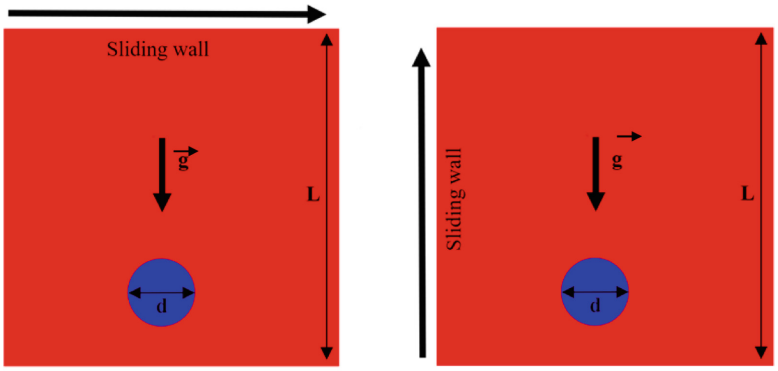

Fig. 1. Initial configuration for the rising numerical domain L = 200 lu, d = 40 lu, (a) the upper wall is moving, (b) the left vertical wall is moving.

2.2 The Pseudopotential Multiple-Relaxation-Time Lattice Boltzmann Model

In this work, the lattice Boltzmann method is employed for simulating the bubble motion in a liquid with a large liquid-gas density ratio and the improved pseudopotential multiphase method is introduced in this section. Initially, the density function distribution with MRT collision operator is given by the following equation [17]:

$$f_\alpha(\boldsymbol{x}+\boldsymbol{e_\alpha}\delta_t, t+\delta_t) = f_\alpha(\boldsymbol{x}, t) - \overline{\Lambda}_{\alpha\beta}\left(f_\beta(\boldsymbol{x}, t) - f_\beta^{(eq)}(\boldsymbol{x}, t)\right) + \delta_t \boldsymbol{F}'_{\boldsymbol{\alpha}}(\boldsymbol{x}, t) \quad (1)$$

$f_\alpha(\boldsymbol{x}, t)$ is the density distribution function, and $f_\beta^{(eq)}(\boldsymbol{x}, t)$ is the equilibrium distribution function. δ_t is the time step, and $\overline{\Lambda}_{\alpha\beta} = \boldsymbol{M}^{-1}\Lambda\boldsymbol{M}$ is the collision matrix, in which $\boldsymbol{M}$ is an orthogonal transformation matrix, and Λ is a diagonal relaxation matrix, and $\boldsymbol{F}'_{\boldsymbol{\alpha}}$ is the forcing term [16].

The distribution function in velocity space is related to the one in momentum space through the MRT operators, $\mathbf{m} = \mathbf{M}.\mathbf{f}$ and $\mathbf{m}^{\mathrm{eq}} = \mathbf{M}.\mathbf{f}^{\mathrm{eq}}$. $\left(\boldsymbol{I} - \frac{\Lambda}{2}\right)\boldsymbol{S} = M\,\boldsymbol{F}'$ is the total force in the moment space. For thermodynamic consistency and mechanical stability under high density ratio of the two-phase flow process, the improved MRT forcing scheme is used [16].

$$f_\alpha(\boldsymbol{x}+\boldsymbol{e_\alpha}\delta_t, t+\delta_t) = f_\alpha(\boldsymbol{x}, t) - \overline{\Lambda}_{\alpha\beta}\left(f_\beta(\boldsymbol{x}, t) - f_\beta^{(eq)}(\boldsymbol{x}, t)\right) + \delta_t \boldsymbol{F}'_{\boldsymbol{\alpha}}(\boldsymbol{x}, t) \quad (2)$$

where $S_1 = \left(\gamma|\boldsymbol{F_{int}}|^2\right)/\left(\psi^2\delta_t(\tau_e - 0.5)\right)$, $S_2 = \left(\gamma|\boldsymbol{F_{int}}|^2\right)/\left(\psi^2\delta_t(\tau_\zeta - 0.5)\right)$.

F is the total force which incorporates the inter-particle interaction force F_{int} and the gravitational force F_g.

The interparticle interaction force that is responsible for the phase separation is defined as [18]:

$$F_{int}(\boldsymbol{x}) = -\psi(\boldsymbol{x})\sum_{x'} G(\boldsymbol{x}, \boldsymbol{x}').\psi(\boldsymbol{x}').(\boldsymbol{x}' - \boldsymbol{x}) \quad (3)$$

$\psi(\mathbf{x})$ represents the effective mass given as a function of local density and the following equation of state is used [16]:

$$\psi(\rho(\boldsymbol{x})) = \sqrt{\frac{2\left(p_{EOS} - \rho c_s^2\right)}{\mathrm{Gc}}} \tag{4}$$

In Eq. (4), p_{EOS} is the pressure calculated via Ping-Robinson equation of state [19]:

$$p_{EOS} = \frac{\rho RT}{1 - b\rho} - \frac{a\rho^2\phi_0(T)}{1 + 2b\rho - b^2\rho^2} \tag{5}$$

$\phi_0(\mathrm{T}) = [1 + (0.37464 + 1.54226\omega - 0.26992\omega^2)\,(1 - \sqrt{T/T_c})]^2$, with ω being the acentric factor which equals 0.344 in the case of water [9].

The gravity force has different formulations the most suitable is [19]:

$$F_g(\boldsymbol{x}) = (\rho(\boldsymbol{x}) - \rho_{ave})g \tag{6}$$

where $\boldsymbol{g}$ is the gravity acceleration and ρ_{ave} is the average density over the physical domain.

The macroscopic properties such as fluid density and velocity are obtained from [20] as:

$$\rho = \sum_i f_i; \quad \rho \boldsymbol{U} = \sum_i \boldsymbol{e_i} f_i + \frac{\delta t}{2} F \tag{7}$$

The boundary conditions for a mobile wall are given through Zou and He [21] approaches, where the rigid walls are dealt through bounce back scheme.

The strength of the external fluid flow is expressed by the Reynolds number as:

$$Re = \frac{V_{lid} \times L}{\nu} \tag{8}$$

3 Numerical Code Validation

To validate the in-house numerical code, the classic 2D wall-driven cavity flow has been analyzed at Reynolds 1000. The velocity profiles along the horizontal line, at y = 0.5, are presented in Fig. 2 for validation purpose and show a fair agreement with the results by Ghia et al. [22], which underpins the applicability of the LBM model used for investigating the other flow configurations explored. Furthermore, to assess the validity of two-phase flow via the MRT pseudopotential lattice Boltzmann method, the Maxwell construction curve is used, depicting the numerical results versus the analytical solution, as shown in Fig. 3. This comparison also shows a good accord between the numerical and the analytical results.

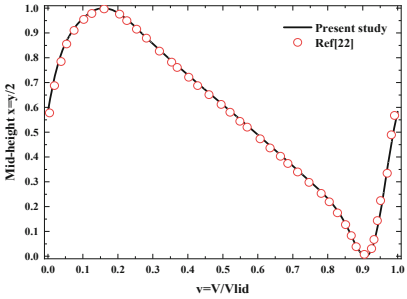

Fig. 2. Comparison of the velocity profiles between the computed results, and the data from reference [22] for Re = 1000.

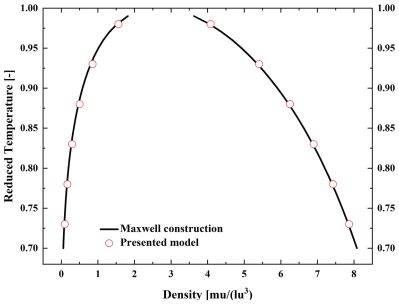

Fig. 3. Maxwell construction obtained by LBM simulation and analytical approach.

4 Result and Discussion

The time evolutions of the flow and density fields are shown in Fig. 4, where the effect of the Reynolds number on the wall-driven flow is illustrated for both configurations. The captures in Fig. 4-1, represent the steady state solutions in the case where the flow is generated by the upper driven-wall. For Re = 300, the competition between the shear and gravitational forces leads to an equilibrium state of the bubble in the upper right side of the cavity as illustrated in Fig. 4-1-a. However, when the fluid flow magnitude increases, the shear force outweighs the gravitational one as shown in Fig. 4-1-b and 1-c respectively for Re = 600 and 900. For this case, the bubble settles in the central region of the square cavity. When the wall-driven is the left vertical one, the flow field structures are overall different from those generated by the horizontal lid-driven wall. In Fig. 4-2-a, it can be seen that the bubble is located near the moving wall, in the upper-right corner at Re = 300, dividing the secondary vortex into several small vortices around the bubble interface. Note also the change in the shape of the bubble in comparison with that described in Fig. 4-1-a. The cases with the remaining Reynolds numbers (Re = 600 and

Re = 900), depicted in Fig. 4-2-b and 2-c, show different flow structures compared to those of Fig. 4-1-a and 1-b generated by the driven upper wall configuration. However, in terms of bubble position, the latter remains localized in the central part of the cavity, i.e. its location is not very affected by the driven wall at high Reynolds numbers. It is obvious to conclude that, the effect of the shear forces generated by the driven walls exceeds that of the buoyant force at Reynolds 600 and 900. However, at the Reynolds number value 300, the competition between both forces brings the bubble to equilibrium near the upper right region for the two configurations.

To add a complement and confirm the previous results, the bubble centroid trajectory has been used to track the bubble's movement inside the square cavity for different Reynolds numbers and both configurations. The effect of the flow strength on the bubble motion is depicted in Fig. 5 where the time step between each point is 200 ts. For the case of the upper driven wall, the bubble mostly follows similar paths with different slopes during the rise process. Once the bubble reaches the upper right corner, it stays there for Re = 300 but for the higher values of this parameter it is pushed downward under the effect of the intense flow. In fact, the competition between the existed forces leads to different terminal bubble placements. As the flow strength increases, the bubble ends up reaching its equilibrium state near the center of the primary vortex, which is located approximately in the center of the square cavity. In contrast, when the bubble is subjected to the effect of the fluid flow generated by the left driven-wall at Re = 300, the bubble is driven upward almost vertically at the beginning. Then, it is driven toward the right upper corner by the peripheral lines of the main cell to its state of equilibrium. For the remaining values of Re (Re = 600 and Re = 900), the slope during the rising process is more titled and the bubble, unlike the previous case, barely exceeds the half height of the square cavity. Moreover, the bubble quickly settles in the middle of the cavity. Therefore, from the above results, it can be concluded that the flow strength outdoes the gravitational acceleration by defining the bubble trajectory.

5 Conclusion

The motion of a buoyant bubble in a single wall-driven square cavity has been studied using the Boltzmann pseudopotential lattice MRT method, where the effects of the wall-driven configurations, and the Reynolds number are considered. The terminal position of the bubble is defined by the interaction between the gravitational and flow strength resulting from the moving side. At high Reynolds numbers, the flow strength overrides buoyancy by inducing the bubble to dwell in the center of the primary vortex. At Re = 300, the bubble reaches its equilibrium state in the upper right corner of the square cavity. Given the results, the trajectory of the bubble's center is found to be sensitive to the position of the mobile wall. The movable left wall configuration reduces the effect of gravitational forces and promotes the impact of the fluid flow strength on the bubble trajectory.

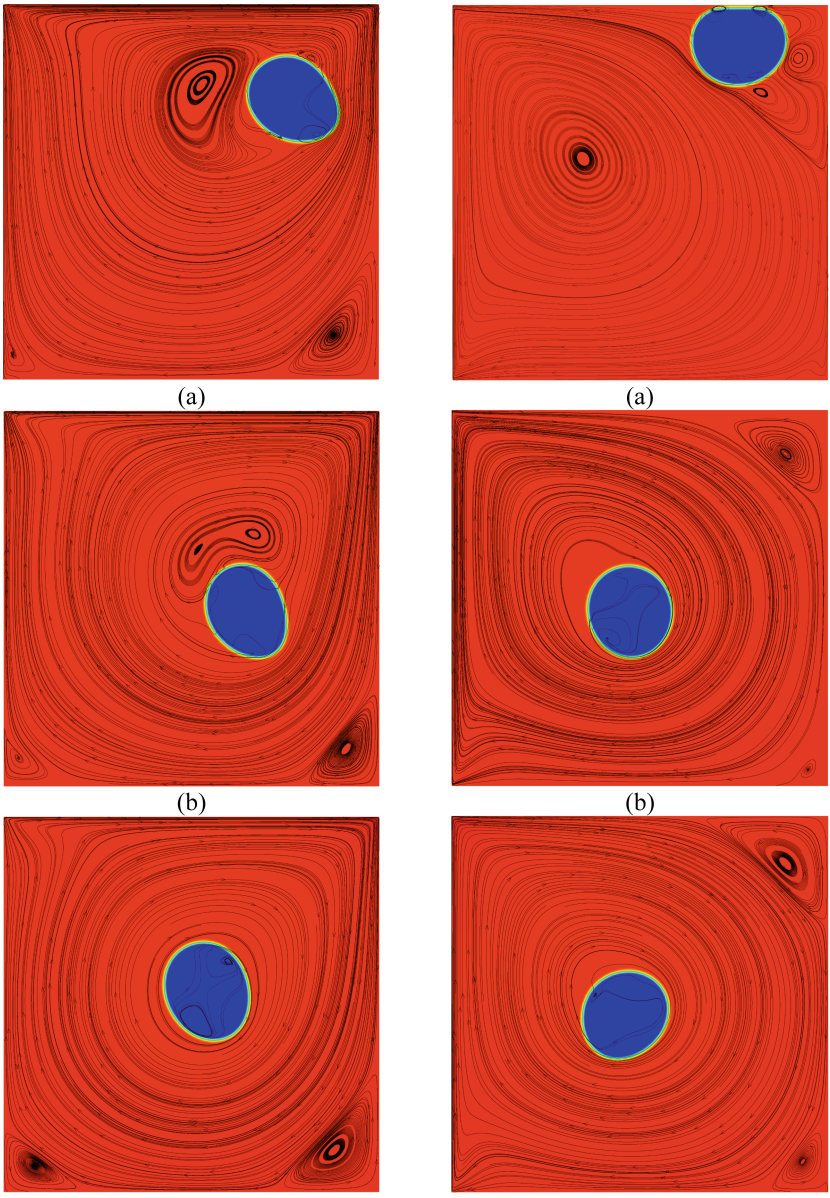

Fig. 4. Steady flow fields and final location of the bubble for different Reynolds numbers, and wall-driven positions, (1) upper wall, (2) left wall: (a) $Re = 300$, (b) $Re = 600$, (c) $Re = 900$.

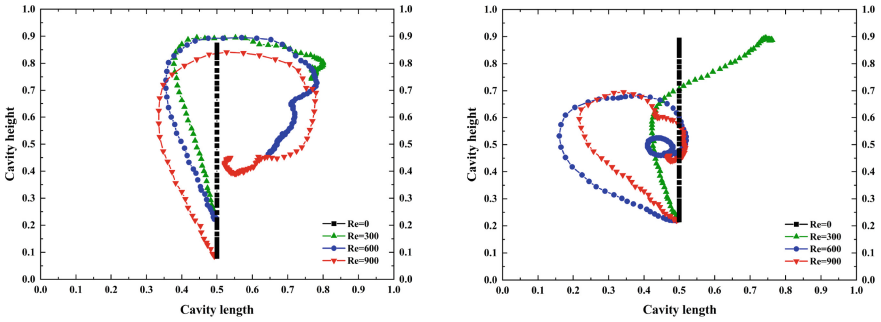

Fig. 5. Trajectories of the bubble moving in the square cavity for various Reynolds numbers: (1) upper wall moving and (2) left wall moving.

References

1. Maytorena, V.M., Hinojosa, J.F.: Three-dimensional numerical study of direct steam generation in vertical tubes receiving concentrated solar radiation. Int. J. Heat Mass Transf. **137**, 413–433 (2019)
2. ben Taher, M.A., Benseddik, Z., Afass, A., Smouh, S., Ahachad, M., Mahdaoui, M.: Energy life cycle cost analysis of various solar water heating systems under Middle East and North Africa region. Case Stud. Thermal Eng. **27**, 101262 (2021)
3. Sarmouk, M.D.-E., Smaili, A., Fellouah, H., Merabtine, A.: Experimental and numerical investigations of a solar space heating system based on design of experiments method. Solar Energy **216**, 396–410 (2021)
4. Wang, J., Han, Z., Liu, Y., Zhang, X., Cui, Z.: Thermodynamic analysis of a combined cooling, heating, and power system integrated with full-spectrum hybrid solar energy device. Energy Convers. Manage. **228**, 113596 (2021)
5. Kulkarni, G.N., Kedare, S.B., Bandyopadhyay, S.: Optimization of solar water heating systems through water replenishment. Energy Convers. Manage. **50**(3), 837–846 (2009)
6. Pal, R.K., Ravi Kumar, K.: Thermo-hydrodynamic modeling of flow boiling through the horizontal tube using Eulerian two-fluid modeling approach. Int. J. Heat Mass Transf. **168**, 120794 (2021)
7. Sallam, S., Taqi, M.: Thermohydraulic behavior of the liquid–vapor flow in the receiver tube of a solar parabolic trough collector. J. Heat Transf. **142**(10) (2020)
8. Dinsenmeyer, R., Fourmigué, J.F., Caney, N., Marty, P.: Volume of fluid approach of boiling flows in concentrated solar plants. Int. J. Heat Fluid Flow **65**, 177–191 (2017)
9. Gong, S., Cheng, P.: Numerical investigation of droplet motion and coalescence by an improved lattice Boltzmann model for phase transitions and multiphase flows. Comput. Fluids **53**, 93–104 (2012)
10. Baroudi, L., Lee, T.: Simulation of a bubble rising at high Reynolds number with mass-conserving finite element lattice Boltzmann method. Comput. Fluids **220**, 104883 (2021)
11. Zhao, W., Liang, J., Sun, M., Wang, Z.: Investigation on the effect of convective outflow boundary condition on the bubbles growth, rising and breakup dynamics of nucleate boiling. Int. J. Therm. Sci. **167**, 106877 (2021)
12. Derfoufi, S., Moufekkir, F., Mezrhab, A.: Numerical assessment of the mixed convection and volumetric radiation in a vertical channel with MRT-LBM. Int. J. Numer. Methods Heat Fluid Flow (2018)

13. Derfoufi, S., Moufekkir, F., Mezrhab, A.: Computation of mixed convection and volumetric radiation in vertical channel based on hybrid thermal lattice Boltzmann method. J. Heat Transf. **138**(9) (2016)
14. Lamarti, H., Mahdaoui, M., Bennacer, R., Chahboun, A.: Numerical simulation of mixed convection heat transfer of fluid in a cavity driven by an oscillating lid using lattice Boltzmann method. Int. J. Heat Mass Transf. **137**, 615–629 (2019)
15. Shan, X., Chen, H.: Lattice Boltzmann model for simulating flows with multiple phases and components. Phys. Rev. E **47**(3), 1815 (1993)
16. Li, Q., Luo, K.H., Li, X.J.: Lattice Boltzmann modeling of multiphase flows at large density ratio with an improved pseudopotential model. Phys. Rev. E **87**(5), 053301 (2013)
17. Zhao, W., Gao, Y., Li, R., Qiu, S., Zhang, Y., Xu, B.: Hybrid phase-change lattice Boltzmann simulation of vapor condensation on vertical subcooled walls. J. Heat Transfer **142**(4), 044503 (2020)
18. Zhao, W., Zhang, Y., Xu, B., Li, P., Wang, Z., Jiang, S.: Multiple-relaxation-time lattice Boltzmann simulation of flow and heat transfer in porous volumetric solar receivers. J. Energy Resour. Technol. **140**(8) (2018)
19. Afass, A., Derfoufi, S., Ahachad, M., Bahraoui, F., Mahdaoui, M.: Wettability effect on homogenous cavitation induced by lid-driven flow. In: 9th international renewable and sustainable energy conference, pp. 1–5. IEEE (2021)
20. Zhao, W., Zhang, Y., Xu, B.: An improved pseudopotential multi-relaxation-time lattice Boltzmann model for binary droplet collision with large density ratio. Fluid Dyn. Res. **51**(2), 025510 (2019)
21. Zou, Q., He, X.: On pressure and velocity boundary conditions for the lattice Boltzmann BGK model. Phys. Fluids **9**(6), 1591–1598 (1997)
22. Ghia, U., Ghia, K.N., Shin, C.T.: High-resolutions for incompressible flow using the Navier-Stokes equations and a multigrid method. J. Comput. Phys. **48**(3), 387–411 (1982)